Journal of Applied Mechanics Vol. 6, pp. 513-520 (August 2003) JSCE

Bifurcation analysis of diffuse modes by the subloading surface model with tangential stress rate effect

Koichi HASHIGUCHI*, Mehdi KHOJASTEHPOUR**

* Dr. of Eng and Dr. of Agr., Professor, Dept. Prod. Environment. Sci., Kyushu University, Hakozaki, Higashi-ku, Fukuoka 812-8581
** M. of Agr., Dept. Prod. Environment. Sci., Kyushu University, Hakozaki, Higashi-ku, Fukuoka 812-8581

The tangential-subloading surface model is capable of describing the plastic strain rate due to the rate of stress inside the yield surface and the inelastic strain rate due to the stress rate component tangential to the subloading surface. The diffuse bifurcation modes of the rectangular specimen subjected to the plane strain loading is analyzed by adopting the tangential-subloading surface model, exhibiting the characteristic regimes of the governing equations (elliptic, hyperbolic and parabolic) in this article. In each of these regimes both symmetric and anti-symmetric diffuse bifurcation modes are available. Besides, the tangential strain rate makes the inception of bifurcation modes easier in not only normal-yield but also subyield states.

Key words: bifurcation, constitutive equation, elastoplasticity, subloading surface mode

1. Introduction

Plastic instability phenomenon is one of the important problems in geomechanics in relation with the progressive failure of geostructure. It is induced by the material softening and geometrical nonlinearity and leads to the *bifurcation of deformation* such as diffuse geometric modes (bulging and buckling) and localized modes (shear band).

Various analytical and computational approaches for the bifurcation of solids have been attempted up to the present[1)-5)]. These results suggest the deficiency of the traditional elastoplastic constitutive equations in which the plastic strain rate is independent of the stress rate component tangential to the yield/loading surface, whilst let the stress rate component tangential to the yield/loading surface and its influence on the inelastic strain rate be called the *tangential stress rate* and the *tangential stress rate effect*. The disregard of the tangential stress rate effect leads to predict unrealistically stiff response of materials when a loading path deviates from the proportional loading, whilst the tangential stress rate effect has been experimentally verified[6)].

Various elastoplastic constitutive equations extended so as to describe the tangential stress rate effect have been proposed up to the present[7)-10)]. Among them, however, only the subloading surface model with tangential stress rate effect[7)] would be applicable to arbitrary loading process including an unloading and a reloading processes, fulfilling the mechanical requirements for constitutive equations[11)-13)], i.e. the continuity condition, the smoothness condition, the Masing effect and the work rate-stiffness relaxation. It is formulated by introducing the additional stain rate, named *tangential strain rate*, induced by the *deviatoric tangential stress rate* into the subloading surface model[14)-17)]. It is of simple form of rate-linearity enabling the reciprocal expression, i.e. the analytical expression of strain rates in terms of stress rate and its inverse expression, and keeps the symmetry of the stiffness modulus, and thus leading to the convenience in the analyses of boundary value problems. Based on the constitutive equation, Hashiguchi and Tsutsumi[18)] derived the condition for the inception of the shear band in the undrained plane strain of soils.

In this article, the constitutive equation of soils will be first reviewed briefly, in which the material functions of soils are incorporated into the subloading surface model with the tangential stress rate effect. It would be applicable to soils in not only normal-yield but also subyield states for not only lower but also higher stress ratio than the critical state. Then, based on the constitutive equation, the diffuse bifurcation modes of the rectangular specimen under the undrained plane strain condition are analyzed and the characteristic regimes of the governing equations depending on the state of stress and material parameters are identified as elliptic, hyperbolic or parabolic regimes leading to the appropriate eigenvalue equations. In each of these regimes both symmetric and anti-symmetric diffuse bifurcation modes are available.

2. Outline of the Subloading Surface Model with Tangential Stress Rate Effect

Denoting the current configuration of material particle as $\mathbf{x}$ and the current velocity as $\mathbf{v}$, the velocity gradient is described as $\mathbf{L} = \partial \mathbf{v}/\partial \mathbf{x}$, by which the strain rate and the continuum spin are defined as $\mathbf{D}(=(\mathbf{L}+\mathbf{L}^{\mathrm{T}})/2)$ and $\mathbf{W}(=(\mathbf{L}-\mathbf{L}^{\mathrm{T}})/2)$, respectively, $(\ )^{\mathrm{T}}$ standing for the transpose.

Now let it be assumed that the strain rate $\mathbf{D}$ is additively

decomposed into the elastic strain rate $\mathbf{D}^e$ and the inelastic strain rate $\mathbf{D}^i$, i.e.

$$\mathbf{D} = \mathbf{D}^e + \mathbf{D}^i, \tag{1}$$

where the elastic strain rate $\boldsymbol{D}^e$ is given by

$$\mathbf{D}^e = \mathbf{E}^{-1}\overset{\circ}{\boldsymbol{\sigma}}. \tag{2}$$

$\boldsymbol{\sigma}$ is the Cauchy stress and $(\circ)$ indicates the proper corotational rate with the objectivity and the fourth-order tensor $\mathbf{E}$ is the elastic modulus. Further, let the inelastic strain rate $\mathbf{D}^i$ be additively decomposed into the *normal-plastic strain rate* $\mathbf{D}^p$ and the *tangential strain rate* $\mathbf{D}^t$, which are induced by the stress rate components normal and tangential, respectively, to the subloading surface, called the *normal* and the *tangential stress rates*, respectively, i.e.

$$\mathbf{D}^i = \mathbf{D}^p + \mathbf{D}^t, \tag{3}$$

Here, it is assumed that the tangential stress rate component inducing the tangential strain rate $\mathbf{D}^t$ is deviatoric stress, obeying the Rudnicki and Rice's conclusion[8] that "no vertex can result from hydrostatic stress increments" based on the consideration of the sliding mechanism in the fissure model. Let $\mathbf{D}^p$ and $\mathbf{D}^t$ be formulated in this section.

2.1 Normal-plastic strain rate due to the subloading surface model

Let it be postulated that the normal-plastic strain rate is given by the subloading surface model with the *smooth elastic-plastic transition*[15]. Then, this model is reviewed briefly. Assume the yield condition:

$$f(\boldsymbol{\sigma}) = F(H). \tag{4}$$

The scalar H is the isotropic hardening/softening variable. Let it be assumed that the function f is homogeneous of degree one in the tensor $\boldsymbol{\sigma}$, satisfying $f(s\boldsymbol{\sigma}) = sf(\boldsymbol{\sigma})$ for any nonnegative scalar s. Here, assume that the evolution of internal structure of materials is caused by the normal-plastic strain rate $\mathbf{D}^p$ and thus the evolution equation of H is homogeneous of degree one in $\mathbf{D}^p$. Then, assume that it is linear function of $\mathbf{D}^p$, i.e.

$$\dot{H} = \mathrm{tr}\{\boldsymbol{f}_h(\boldsymbol{\sigma}, H)\mathbf{D}^p\}. \tag{5}$$

where $\boldsymbol{f}_h$ is the second-order tensor, $(\dot{\bullet})$ stands for the material-time derivative and tr( ) is the trace.

Hereinafter, the elastoplastic constitutive equation will be formulated in the framework of the *unconventional plasticity*[17] as the extended plasticity theory such that the interior of the yield surface is not a purely elastic domain but a plastic deformation is induced by the rate of stress inside the yield surface. Thus, the conventional yield surface is renamed as the *normal-yield surface*, since its interior is not regarded as a purely elastic domain in the present model.

Now, let the *subloading surface* be introduced, which always passes through the current stress point $\boldsymbol{\sigma}$ and also keeps the similar shape to the normal-yield surface and the positioning of similarity to the normal-yield surface with respect to the origin of stress space, i.e. $\boldsymbol{\sigma} = 0$. The approaching degree to the normal-yield state can be described by the ratio of the size of the subloading surface to that of the normal-yield surface, i.e. the similarity-ratio R of these surfaces, while $R = 0$ corresponds to the most elastic state in which the stress coincides with the similarity-center and $R = 1$ to the normal-yield state in which the stress exists on the normal-yield surface. Hereinafter, let the similarity-ratio R be called *the normal-yield ratio*. Then, the subloading surface is described as

$$f(\boldsymbol{\sigma}) = RF(H). \tag{6}$$

The normal-yield and subloading surfaces are illustrated in Fig. 1, where $\boldsymbol{\sigma}_y (= \boldsymbol{\sigma}/R)$ on the normal-yield surface is the conjugate stress of the current stress $\boldsymbol{\sigma}$ on the subloading surface.

The time-differentiation of Eq. (6) is given as

$$\mathrm{tr}\left(\frac{\partial f(\boldsymbol{\sigma})}{\partial \boldsymbol{\sigma}}\overset{\circ}{\boldsymbol{\sigma}}\right) = \dot{R}F + RF'\dot{H}, \tag{7}$$

where

$$F' \equiv \frac{dF}{dH}. \tag{8}$$

It is observed from experiments that the stress asymptotically approaches to the normal-yield surface in the plastic loading process $\mathbf{D}^p \neq 0$. Thus, let the following evolution equation of the normal-yield ratio R be assumed.

$$\dot{R} = U\|\mathbf{D}^p\| \quad \text{for } \mathbf{D}^p \neq 0, \tag{9}$$

where U is the monotonically decreasing function of the normal-yield ratio R, satisfying

$$U = \begin{cases} \infty & \text{for } R = 0, \\ 0 & \text{for } R = 1, \end{cases} \qquad (U < 0 \text{ for } R > 1). \tag{10}$$

$\|\ \|$ stands for the magnitude. Let the function U satisfying Eq. (10) be simply given by

$$U = -u_R \ln R, \tag{11}$$

where u_R is a material constant prescribing the approaching rate of the current stress to the normal-yield surface with a plastic deformation.

Substitution of Eq. (9) into Eq. (7) leads to the *extended consistency condition* for the subloading surface:

$$\mathrm{tr}\left(\frac{\partial f(\boldsymbol{\sigma})}{\partial \boldsymbol{\sigma}}\overset{\circ}{\boldsymbol{\sigma}}\right) = U\|\mathbf{D}^p\|F + RF'\dot{H}. \tag{12}$$

Assume the associated flow rule

$$\mathbf{D}^p = \lambda \mathbf{N} \ (\lambda > 0), \tag{13}$$

where

$$\mathbf{N} \equiv \frac{\partial f(\boldsymbol{\sigma})}{\partial \boldsymbol{\sigma}} \Big/ \left\| \frac{\partial f(\boldsymbol{\sigma})}{\partial \boldsymbol{\sigma}} \right\| \quad (\|\mathbf{N}\| = 1). \tag{14}$$

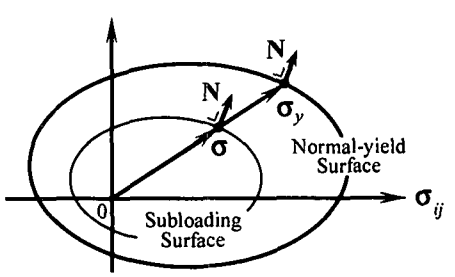

Fig. 1. Normal-yield and subloading surfaces

Substitution of Eq. (13) into Eq. (12) leads to

$$\lambda = \frac{\mathrm{tr}(\mathbf{N}\mathring{\boldsymbol{\sigma}})}{M_p}, \tag{15}$$

where

$$M_p \equiv \left(\frac{F'}{F}h + \frac{U}{R}\right)\mathrm{tr}(\mathbf{N}\boldsymbol{\sigma}), \tag{16}$$

h is function of the stress, plastic internal variables and $\mathbf{N}$ in degree one, which is related to $\dot{H}$ as

$$h \equiv \mathrm{tr}(f_h\mathbf{N}) = \dot{H}/\lambda = \dot{H}/\|\mathbf{D}^p\|. \tag{17}$$

since the rates of internal variables include λ in degree one.

The plastic strain rate (13) with Eqs. (15) and (16) is obtained by substituting the associated flow rule (13) into the extended consistency condition obtained by incorporating the evolution rule (9) of the normal-yield ratio R into the time-differentiation of Eq. (7) for the subloading surface. Then, the plastic loading process develops gradually as the stress approaches the normal-yield surface, exhibiting a *smooth elastic-plastic transition*. Thus, the subloading surface model fulfills the *smoothness condition*[11)-13)].

2.2 Extension to tangential stress rate effect

Noting that the tangential strain rate $\mathbf{D}^t$ as well as the plastic strain rate $\mathbf{D}^p$ would not be induced in the state $R = 0$ but would be gradually induced as the stress approaches the normal-yield surface, let the tangential strain rate $\mathbf{D}^t$ be formulated as

$$\mathbf{D}^t = \frac{1}{T}\mathring{\boldsymbol{\sigma}}_t^*, \tag{18}$$

where T is a monotonically decreasing function of R satisfying the following condition.

$$T = \begin{cases} \infty & \text{for } R = 0, \\ \xi & \text{for } R = 1. \end{cases} \tag{19}$$

ξ being a material function of the stress and the plastic internal variables in general. The function T, called the *tangential inelastic modulus*, satisfying Eq. (19) is simply given by

$$T = \xi R^{-b} \tag{20}$$

where $b\,(\geq 1)$ is a material constant. The second-order tensor $\mathring{\boldsymbol{\sigma}}_t^*$ is given as follows:

$$\mathring{\boldsymbol{\sigma}}^* = \mathring{\boldsymbol{\sigma}}_n^* + \mathring{\boldsymbol{\sigma}}_t^*, \tag{21}$$

$$\mathring{\boldsymbol{\sigma}}_t^* = \mathring{\boldsymbol{\sigma}}^* - \mathring{\boldsymbol{\sigma}}_n^*, \quad \mathring{\boldsymbol{\sigma}}_n^* = \mathrm{tr}(\mathbf{n}^*\mathring{\boldsymbol{\sigma}}^*)\mathbf{n}^*, \tag{22}$$

$$\mathring{\boldsymbol{\sigma}}^* = \mathring{\boldsymbol{\sigma}} - \dot{\sigma}_m\mathbf{I}, \quad \sigma_m = \frac{1}{3}\mathrm{tr}(\boldsymbol{\sigma}), \tag{23}$$

$$\mathbf{n}^* \equiv \left(\frac{\partial f(\boldsymbol{\sigma})}{\partial \boldsymbol{\sigma}}\right)^* \Big/ \left(\left\|\frac{\partial f(\boldsymbol{\sigma})}{\partial \boldsymbol{\sigma}}\right\|\right)^* \quad (\|\mathbf{n}^*\| = 1). \tag{24}$$

$(\,)^*$ stands for the deviatoric part, $\mathbf{I}$ and $\mathbf{n}^*$ are the identity tensor and the normalized deviatoric outward-normal tensor of the subloading surface, respectively. The stress rate $\mathring{\boldsymbol{\sigma}}_t^*$ is called the *deviatoric tangential stress rate* fulfilling

$$\mathrm{tr}(\mathbf{N}\mathring{\boldsymbol{\sigma}}_t^*) = 0, \quad \mathrm{tr}\mathring{\boldsymbol{\sigma}}_t^* = 0. \tag{25}$$

The deviatoric tangential stress rate $\mathring{\boldsymbol{\sigma}}_t^*$ in the principal stress space is directed toward the tangential line of the closed curve formed by the intersection of the subloading surface and deviatoric stress plane as illustrated in Fig. 2. In addition, let the function T be named the *tangential modulus*. The tangential strain rate $\mathbf{D}^t$ is related linearly to the deviatoric-tangential stress rate $\mathring{\boldsymbol{\sigma}}_t^*$ through the similarity-ratio R so as to exhibit the smooth elastic-inelastic transition. Besides, it can be formulated so as to be hardly induced when a stress lies inside the normal-yield surface by giving a large value to the material parameter b.

The strain rate $\mathbf{D}$ is given as

$$\mathbf{D} = \mathbf{E}^{-1}\mathring{\boldsymbol{\sigma}} + \frac{\mathrm{tr}(\mathbf{N}\mathring{\boldsymbol{\sigma}})}{M_p}\mathbf{N} + \frac{1}{T}\mathring{\boldsymbol{\sigma}}_t^*. \tag{26}$$

Now, let the elastic modulus tensor $\mathbf{E}$ be given by the Hooke's type as

$$E_{ijkl} = (K - \frac{2}{3}G)\delta_{ij}\delta_{kl} + G(\delta_{ik}\delta_{jl} + \delta_{il}\delta_{jk}), \tag{27}$$

where K and G are the elastic bulk and shear moduli, respectively, which are functions of the stress and internal state variables in general and δ_{ij} is the Kronecker's delta, i.e. $\delta_{ij} = 1$ for $i = j$ and $\delta_{ij} = 0$ for $i \neq j$. The inverse expression of Eq. (26) is given as:

$$\begin{aligned}\mathring{\boldsymbol{\sigma}} = \frac{1}{1+2G/T}\Big\{&\mathbf{ED} - \frac{\mathrm{tr}(\mathbf{NED})}{M_p + \mathrm{tr}(\mathbf{NEN})}\Big[\mathbf{EN} \\ &+ \frac{2G}{T}\Big\{\frac{1}{3}\mathrm{tr}(\mathbf{EN})\mathbf{I} - \Big(M_p + \frac{1}{3}\mathrm{tr}\mathbf{N}\,\mathrm{tr}(\mathbf{EN})\Big)\frac{\mathbf{n}^*}{\|\mathbf{N}^*\|}\Big\}\Big] \\ &+ \frac{2G}{T}\mathrm{tr}(\mathbf{ED})\Big(\frac{1}{3}\mathbf{I} - \frac{1}{3}\mathrm{tr}\mathbf{N}\frac{\mathbf{n}^*}{\|\mathbf{N}^*\|}\Big)\Big\}.\end{aligned} \tag{28}$$

Both the plastic strain rate $\mathbf{D}^p$ in Eq. (13) with Eq. (15) and the tangential strain rate $\mathbf{D}^t$ in Eq. (18) with Eq. (20) are formulated so as to be gradually induced as the normal-yield ratio R approaches closely unity, i.e. as the stress approaches closely the normal-yield surface, exhibiting the smooth elastic-inelastic transition and fulfilling the smoothness condition and the *continuity condition*[11)-13)] defined as "the stress rate response changes continuously for a continuous change of the strain rate", which can be expressed mathematically as follows:

$$\lim_{\delta\mathbf{D}\to 0}\mathring{\boldsymbol{\sigma}}(\boldsymbol{\sigma}, \mathbf{S}_t, \mathbf{D} + \delta\mathbf{D}) = \mathring{\boldsymbol{\sigma}}(\boldsymbol{\sigma}, \mathbf{S}_t, \mathbf{D}). \tag{29}$$

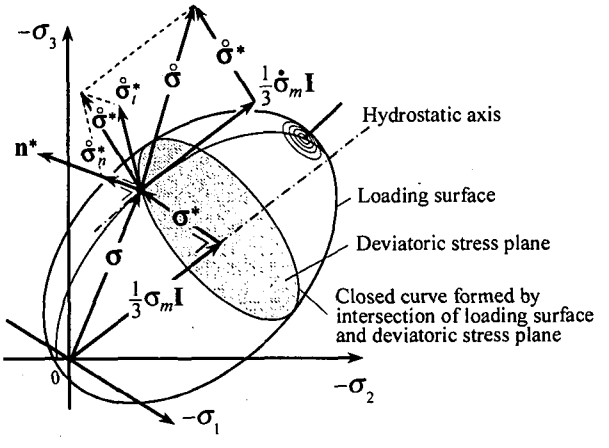

Fig. 2. Deviatoric tangential stress rate $\mathring{\boldsymbol{\sigma}}_t^*$ illustrated in the principle stress space

On the other hand, the extended flow models incorporating the tangential strain rate within the conventional elastoplasticity, e.g. the models of Rudnicki and Rice[8] and Papamichos and Vardoulakis[10] violate this condition for the stress path along the yield surface. Thus, the constitutive equation in Eqs. (26) or (28) would not be required to be limited to a monotonic loading process in the normal-yield state but would be applicable to a general loading process for materials with an arbitrary smooth yield surface.

The positive proportionality factor in the associated flow rule is expressed in terms of the strain rate $\mathbf{D}$, rewriting λ by Λ, as follows:

$$\Lambda = \frac{\mathrm{tr}(\mathbf{NED})}{M_p + \mathrm{tr}(\mathbf{NEN})}, \tag{30}$$

because of $\mathrm{tr}(\mathbf{NE}\mathring{\boldsymbol{\sigma}}_t^*) = 0$ for Eq. (27). Then, let the loading criterion be given by the positiveness of the proportionality factor Λ as follows[13]:

$$\left.\begin{aligned} \mathbf{D}^P \neq 0 &: \Lambda > 0, \\ \mathbf{D}^P = 0 &: \Lambda \leq 0. \end{aligned}\right\} \tag{31}$$

2.3 Material functions for soils

Let the particular forms of the material functions for soils be given in this section. The subloading surface for simple isotropic soils is given as follows:

$$f(\boldsymbol{\sigma}) = P(1+\chi^2), \tag{32}$$

where

$$P \equiv -\frac{1}{3}\mathrm{tr}\boldsymbol{\sigma}, \quad \chi \equiv \|\boldsymbol{\eta}\|/m_c, \tag{33}$$

$$\boldsymbol{\eta} \equiv \boldsymbol{\sigma}^*/P, \quad \boldsymbol{\sigma}^* \equiv \boldsymbol{\sigma} - P\mathbf{I}. \tag{34}$$

m_c is the material constant describing the stress ratio $\|\boldsymbol{\eta}\|$ in the critical state line.

The isotropic hardening/softening function[18] F is given by

$$F = F_0 \exp\left(\frac{H}{\rho - \gamma}\right), \tag{35}$$

where F_0 is the initial value of F. ρ and γ are material constants describing the slope of the normal consolidated curve and the swelling curve, respectively, in the $(\ln v, \ln P)$ plane (v: volume, P: pressure). The evolution equation of the isotropic hardening variable H is given by

$$\dot{H} = -\mathrm{tr}\,\mathbf{D}^P. \tag{36}$$

Let the function U for the evolution rule (9) of the normal-yield ratio R be given by Eq. (11) itself.

Further, we assume the function ξ in the tangential modulus T of Eq. (20) as

$$\xi = \frac{P}{a\chi^c}. \tag{37}$$

a and c are material constants. Then, the tangential inelastic modulus T in Eq. (18) with Eqs. (20) and (37) is formulated to induce the tangential stress rate effect gradually with the increase of χ and/or R, whilst the effect decreases with the increase of pressure. On the other hand, the equation of Yatomi et al.[9] for the tangential inelastic modulus, i.e. $T = C(m - \|\boldsymbol{\eta}\|)P$ (C: material constant) is applicable only to the normal-yield state $R = 1$ under the lower stress ratio than that in the critical state, i.e. $\chi \leq 1$.

The bulk and shear moduli are given as

$$K = \frac{P}{\gamma}, \qquad G = \frac{3(1-2\nu)}{2(1+\nu)}K. \tag{38}$$

where ν is Poisson's ratio.

The concrete form of the plastic modulus in Eq. (16) for isotropic soils is described from Eqs. (32)-(35) as follows:

$$\left.\begin{aligned} M_p &= \left(-u_R \ln R + \frac{R}{\rho-\gamma}\frac{1-\chi^2}{\sqrt{\varsigma}}\right)\frac{F}{\sqrt{\varsigma}}, \\ \varsigma &\equiv \frac{1}{3}A + \left(2\frac{\chi}{m}\right)^2, \quad A \equiv (1-\chi^2)^2. \end{aligned}\right\} \tag{39}$$

Hereafter, the material constants be chosen as $\rho = 0.0924$, $\gamma = 0.0168$, $m_c = 1.17$, $b = 1.0$, $c = 3.0$ and $\nu = 0.333$.

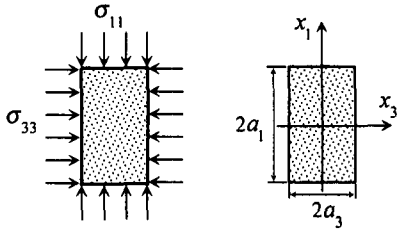

Fig 3. Geometric configuration and the boundary stresses of the sample

Fig. 4. Bifurcation modes: (a) Symmetric mode (bulging), (b) Anti-symmetric mode (buckling)

3. Bifurcation Analysis

The diffuse bifurcation modes are analyzed by the subloading surface model with tangential stress rate effect reviewed in the preceding section.

3.1 Constitutive relations

Consider the deformation of rectangular, homogeneous block subject to continuing biaxial loading of homogeneous normal stress under the undrained plane strain condition in the (x_1, x_3) plane (see Fig. 3) which starts from an isotropically consolidated state. The symmetric and the anti-symmetric modes may be induced as shown in Fig. 4. It holds that

$$\left.\begin{aligned} \mathring{\sigma}_{11} - \mathring{\sigma}_{33} &= 2\mu^*(D_{11} - D_{33}), \\ \mathring{\sigma}_{31} &= 2\mu D_{31}, \end{aligned}\right\} \tag{40}$$

with

$$D_{11} + D_{33} = 0, \quad D_{12} = D_{22} = D_{23} = 0. \tag{41}$$

μ^* and μ which are the instantaneous shear moduli for the normal effective stress difference $\sigma_{11} - \sigma_{33}$ and for shear stress σ_{31}, respectively are derived as follows[18]:

$$\mu^* = G\frac{Mr}{Me} \ (\leq G), \quad \mu = \frac{G}{1+2G/T} \ (\leq G) \tag{42}$$

where

$$M_r \equiv M_p + K\frac{A}{\varsigma}, \quad M_e \equiv M_p + (K - \frac{2}{3}G)\frac{A}{\varsigma} + 2G. \quad (43)$$

Here, it should be noted that the incorporation of the tangential strain rate term has no influence on μ^* but lowers μ involving the function T. The present formulation fulfilling both the continuity and the smoothness conditions is manifested in Fig. 5. On the other hands, in conventional plasticity models with $a = 0$, μ^* and μ suddenly jump from the purely elastic response to the normal-yield response at the moment when the stress reaches the normal-yield surface.

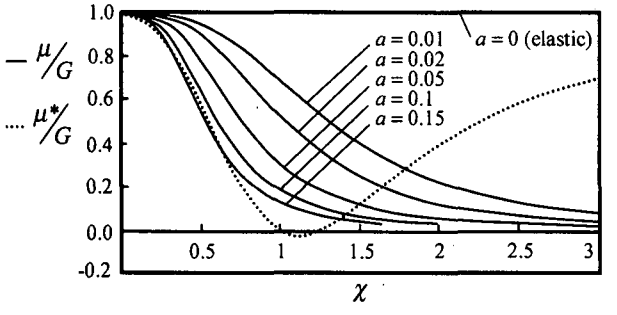

Fig. 5. Instantaneous shear moduli vs. χ

3.2 Field equations

Let diffuse bifurcation condition in the biaxial compression under the undrained plane strain condition be analyzed based on the approach of Hill and Hutchinson[1] that has been done for plastically-incompressible materials in the conventional plasticity. We focus our attention on the behavior of the saturated soils under the undrained condition, and then let the *Cauchy stress tensor* $\boldsymbol{\sigma}$ be meant the *effective Cauchy stress* excluded a pore pressure u from the *total Cauchy stress* $\mathbf{T}$, which is defined by

$$\boldsymbol{\sigma} = \mathbf{T} + u\mathbf{I}. \quad (44)$$

For the plane strain condition using the divergence theorem, the equilibrium equation is obtained as

$$\mathrm{div}\,\dot{\boldsymbol{\Pi}} = \mathbf{0}, \quad (45)$$

$\dot{\boldsymbol{\Pi}}$ is called the *total nominal (first Piola-Kirchhoff) stress rate* that is related to the *total Cauchy stress rate* $\dot{\mathbf{T}}$ by

$$\dot{\boldsymbol{\Pi}} = \dot{\mathbf{T}} + (\mathrm{tr}\mathbf{D})\mathbf{T} - \mathbf{T}\mathbf{L}^{\mathrm{T}}. \quad (46)$$

Since the stress rates $\dot{\mathbf{T}}$ and $\dot{\boldsymbol{\sigma}}$ are not invariant under rigid rotation, let the corresponding *Jaumann rate* be introduced as the objective corotational rates:

$$\mathring{\mathbf{T}} \equiv \dot{\mathbf{T}} + \mathbf{T}\mathbf{W} - \mathbf{W}\mathbf{T}, \quad (47)$$

$$\mathring{\boldsymbol{\sigma}} \equiv \dot{\boldsymbol{\sigma}} + \boldsymbol{\sigma}\mathbf{W} - \mathbf{W}\boldsymbol{\sigma}. \quad (48)$$

Substituting Eqs. (47) and (48) to Eq. (46) with Eq. (44), the total nominal stress rate $\dot{\boldsymbol{\Pi}}$ can be rewritten as

$$\begin{aligned}\dot{\boldsymbol{\Pi}} &= \mathring{\mathbf{T}} + (\mathrm{tr}\mathbf{D})\mathbf{T} - \mathbf{T}\mathbf{D} + \mathbf{W}\mathbf{T} \\ &= \dot{\boldsymbol{\Pi}}' - \dot{u}\mathbf{I} - u(\mathrm{tr}\mathbf{D})\mathbf{I} + u\mathbf{L}^{\mathrm{T}}, \end{aligned} \quad (49)$$

where

$$\dot{\boldsymbol{\Pi}}' = \mathring{\boldsymbol{\sigma}} + (\mathrm{tr}\mathbf{D})\boldsymbol{\sigma} - \boldsymbol{\sigma}\mathbf{D} + \mathbf{W}\boldsymbol{\sigma}. \quad (50)$$

$\dot{\boldsymbol{\Pi}}'$ is called the *effective nominal stress rate*[9]. Using Eq. (45) for continuing linear equilibrium, the total nominal stress rate must satisfy

$$\left.\begin{aligned}\frac{\partial \dot{\Pi}'_{11}}{\partial x_1} + \frac{\partial \dot{\Pi}'_{13}}{\partial x_3} - \frac{\partial \dot{u}}{\partial x_1} = 0, \\ \frac{\partial \dot{\Pi}'_{33}}{\partial x_3} + \frac{\partial \dot{\Pi}'_{31}}{\partial x_1} - \frac{\partial \dot{u}}{\partial x_3} = 0.\end{aligned}\right\} \quad (51)$$

The rates of the nominal stress $\boldsymbol{\Pi}'$ in Eq. (51) are given in terms of the Cauchy stress and the velocity components from Eqs (40) and (50) as follows:

$$\left.\begin{aligned}\dot{\Pi}'_{11} - \dot{\Pi}'_{33} &= (2\mu^* - \sigma)(\frac{\partial v_1}{\partial x_1} - \frac{\partial v_3}{\partial x_3}), \\ \dot{\Pi}'_{13} &= (\mu - \sigma)\frac{\partial v_3}{\partial x_1} + (\mu - \tau)\frac{\partial v_1}{\partial x_3}, \\ \dot{\Pi}'_{31} &= (\mu + \tau)\frac{\partial v_3}{\partial x_1} + (\mu - \sigma)\frac{\partial v_1}{\partial x_3},\end{aligned}\right\} \quad (52)$$

where

$$\sigma = \frac{1}{2}(\sigma_{11} + \sigma_{33}), \quad \tau = \frac{1}{2}(\sigma_{11} - \sigma_{33}). \quad (53)$$

(v_1, v_3) are the (x_1, x_3) -components of velocity.

Now, introduce a stream function $\Psi(x_1, x_3)$ [1] such that

$$v_1 = \frac{\partial \Psi}{\partial x_3}, \qquad v_3 = -\frac{\partial \Psi}{\partial x_1}. \quad (54)$$

The substitution of Eqs. (52) and (54) into Eq. (51) leads to

$$(\mu + \tau)\frac{\partial^4 \Psi}{\partial x_1^4} + 2(2\mu^* - \mu)\frac{\partial^4 \Psi}{\partial x_1^2 \partial x_3^2} + (\mu - \tau)\frac{\partial^4 \Psi}{\partial x_3^4} = 0. \quad (55)$$

3.3 Classification of bifurcation regimes

Consider the rectangular homogeneous specimen, with the current dimensions $2a_1 \times 2a_3$ (see Fig. 3) subject to a current axial stress σ_{11} in the ends and a constant hydrostatic confining pressure $\sigma_{33} = \sigma_c$. We examine the possibility of incremental deformation when the sides (the faces perpendicular to x_3 direction) remain traction-free, the ends are subject to frictionless constrains and the pore water pressure maintains homogeneous. We seek modes of the type

$$\Psi = v(x_3)\cos(n_1 x_1). \quad (56)$$

The substitution of Eq. (56) into Eq. (54) leads to

$$v_1 = v'(x_3)\cos(n_1 x_1), \qquad v_3 = n_1 v(x_3)\sin(n_1 x_1), \quad (57)$$

where $v' = dv_3 / dx_3$. The kinematic constraint on the ends is satisfied when

$$n_1 = m\pi / 2a_1, \quad m = 1, 2, 3, ..., \quad (58)$$

by placing the origin of coordinates at the specimen center when m is odd and at a distance a_1/m from the center when m is even. From Eq. (55), $v(x_3)$ must satisfy

$$(\mu - \tau)v'''' - 2(2\mu^* - \mu)n_1^2 v'' + (\mu + \tau)n_1^4 v = 0. \quad (59)$$

The boundary conditions can be written

$$\left.\begin{aligned}&v_1 = 0, \ \dot{\Pi}'_{31} = 0 && \text{on the ends,} \\ &\dot{\Pi}'_{33} = \dot{u} - \sigma_c \frac{\partial v_3}{\partial x_3}, \ \dot{\Pi}'_{13} = -\sigma_c \frac{\partial v_3}{\partial x_1} && \text{on the sides.}\end{aligned}\right\} \quad (60)$$

Since $\dot{\Pi}'_{31}$ given by Eq. (52) also varies as $\cos(n_1 x_1)$, the smoothness of stress distribution on the ends is automatically satisfied. Substituting Eqs. (40), (41) and (60) into Eq. (51), the boundary conditions on the sides can be expressed

$$\left.\begin{aligned} &v'' + n_1^2 v = 0, \\ &(\mu - \tau)v''' - (4\mu^* - \mu - \tau)n_1^2 v' = 0, \end{aligned}\right\} \quad \text{on } x_3 = \pm a_3. \quad (61)$$

Symmetric modes satisfy $\Psi(x_1, x_3) = -\Psi(x_1, -x_3)$ based on odd functions $v(x_3)$ and anti-symmetric modes satisfy $\Psi(x_1, x_3) = \Psi(x_1, -x_3)$ based on even functions $v(x_3)$.

General solution of Eq. (59) is given in the form

$$v(x_3) = \sum_{j=1}^{4} \mathrm{M}_j \exp(i n_3 x_3), \quad (62)$$

where $i = \sqrt{-1}$. and M_j (j=1, 2, 3, 4) are the real and/or complex constants. Substitution of Eq. (62) into Eq. (59) reveals that n_3 satisfies

$$(\mu + \tau)n_1^4 + 2(2\mu^* - \mu)n_1^2 n_3^2 + (\mu - \tau)n_3^4 = 0. \quad (63)$$

The roots of Eq. (63) are classified into the elliptic complex (EC), the elliptic imaginary (EI), the hyperbolic (H) and the parabolic (P) regimes depending on the current sate of stress and internal variables. In each of these regimes diffuse bifurcations are possible and, in fact, in each regime the analysis leading to the appropriate eigenvalue equation. On the other hand, we can construct functions of each type from solutions of types Eq. (62), and eigenvalue equations corresponding to Eq. (63) in each of four regimes EC, EI, H and P.

(1) Elliptic complex regime (EC)

The elliptic regime can be subdivided into portions where the roots are complex (EC) and imaginary (EI). In the elliptic complex region, the solutions for the symmetric modes are of the form

$$v(x_3) = \mathrm{Re}[\mathrm{M}\sin(n_3 x_3)], \quad (64)$$

where Re[...] denotes the real part of[...], M is a complex constant, and $n_3 = n_1(p \pm iq)$ that $p \pm iq$ are any complex roots of Eq. (63). Similarly, the anti-symmetric modes are of the form

$$v(x_3) = \mathrm{Re}[\mathrm{M}\cos(n_3 x_3)], \quad (65)$$

Substituting Eqs (64) and (65) into boundary conditions (61) lead to an eigenvalue equation of the form

$$\frac{q\sin(2pn_1a_3)}{p\sinh(2qn_1a_3)} = \pm \frac{\left(\frac{\mu/\tau - 1}{\mu/\tau + 1}\right)^{1/2} + (2\mu^*/\tau - 1)}{\left(\frac{\mu/\tau - 1}{\mu/\tau + 1}\right)^{1/2} - (2\mu^*/\tau - 1)}, \quad (66)$$

where the (+) sign applies for the symmetric modes, and the (-) sign applies for the anti-symmetric modes. For both the symmetric and anti-symmetric modes, the real and imaginary parts, p and q satisfy the following equations:

$$\left.\begin{aligned} p^2 + q^2 &= \left(\frac{\mu/\tau + 1}{\mu/\tau - 1}\right)^{1/2}, \\ p^2 - q^2 &= \frac{2\mu^*/\mu - 1}{\tau/\mu - 1}. \end{aligned}\right\} \quad (67)$$

(2) Elliptic imaginary regime (EI)

In the elliptic imaginary regime, there are symmetric modes of the form

$$v(x_3) = \mathrm{M}\sinh(pn_1x_3) + \mathrm{N}\sinh(qn_1x_3), \quad (68)$$

and anti-symmetric modes are of the form

$$v(x_3) = \mathrm{M}\cosh(pn_1x_3) + \mathrm{N}\cosh(qn_1x_3), \quad (69)$$

where both M and N are the real constants now. p and q are positive and related to the coefficients of Eq. (63). In the elliptic imaginary regime, the roots of Eq. (63) have the form $\pm ip$ and $\pm iq$. The substitution of Eq. (68) into the boundary conditions (61) yields the eigenvalue equation for symmetric modes:

$$\frac{p\tanh(qn_1a_3)}{q\tanh(pn_1a_3)} = \left(\frac{p^2 + 1}{q^2 + 1}\right)^2, \quad (70)$$

Repeating this for the anti-symmetric modes (69) gives

$$\frac{p\tanh(pn_1a_3)}{q\tanh(qn_1a_3)} = \left(\frac{p^2 + 1}{q^2 + 1}\right)^2, \quad (71)$$

where p and q for both the symmetric and anti-symmetric modes, satisfy the following equations:

$$\left.\begin{aligned} \frac{1}{2}(p^2 + q^2) &= -\frac{2\mu^*/\mu - 1}{\tau/\mu - 1}, \\ \frac{1}{2}(p^2 - q^2) &= -\frac{\left((2\mu^*/\mu - 1)^2 + (\tau/\mu)^2 - 1\right)^{1/2}}{\tau/\mu - 1}. \end{aligned}\right\} \quad (72)$$

(3) Hyperbolic regime (H)

In the hyperbolic regime the appropriate symmetric modes are

$$v(x_3) = \mathrm{M}\sin(pn_1x_3) + \mathrm{N}\sin(qn_1x_3), \quad (73)$$

and the appropriate anti-symmetric modes are

$$v(x_3) = \mathrm{M}\cos(pn_1x_3) + \mathrm{N}\cos(qn_1x_3), \quad (74)$$

where p and q are positive roots of Eq. (63). The substitution of Eqs. (73) and (74) into the boundary conditions (61) yields the eigenvalue equation for symmetric modes

$$\frac{q\tan(pn_1a_3)}{p\tan(qn_1a_3)} = \left(\frac{q^2 - 1}{p^2 - 1}\right)^2, \quad (75)$$

and for anti-symmetric modes

$$\frac{q\tan(qn_1a_3)}{p\tan(pn_1a_3)} = \left(\frac{q^2 - 1}{p^2 - 1}\right)^2, \quad (76)$$

where p and q for both the symmetric and anti-symmetric modes, satisfy the following equations:

$$\left.\begin{aligned} \frac{1}{2}(p^2 + q^2) &= \frac{2\mu^*/\mu - 1}{\tau/\mu - 1}, \\ \frac{1}{2}(p^2 - q^2) &= -\frac{\left((2\mu^*/\mu - 1)^2 + (\tau/\mu)^2 - 1\right)^{1/2}}{\tau/\mu - 1}. \end{aligned}\right\} \quad (77)$$

(4) Parabolic regime (P)

In the parabolic regime one pair of roots of Eq. (63) consists of real roots, and the other pair is consists of imaginary roots. With p and iq, the positive real and imaginary roots, respectively, the symmetric modes in the parabolic regime are of the form

$$v(x_3) = \mathrm{M}\sin(pn_1x_3) + \mathrm{N}\sinh(qn_1x_3), \tag{78}$$

and the anti-symmetric modes are given by

$$v(x_3) = \mathrm{M}\cos(pn_1x_3) + \mathrm{N}\cosh(qn_1x_3), \tag{79}$$

The substitution of Eqs. (78) and (79) into the boundary conditions (61) yields the eigenvalue equation for symmetric modes

$$\frac{q\tan(pn_1a_3)}{p\tanh(qn_1a_3)} = \left(\frac{q^2+1}{p^2-1}\right)^2, \tag{80}$$

and for anti-symmetric modes

$$\frac{q\tanh(qn_1a_3)}{p\tan(pn_1a_3)} = -\left(\frac{q^2+1}{p^2-1}\right)^2, \tag{81}$$

where p and q for both the symmetric and anti-symmetric modes, satisfy the following equations:

$$\left.\begin{aligned}\frac{1}{2}(p^2+q^2) &= \frac{\left((2\mu^*/\mu-1)^2+(\tau/\mu)^2-1\right)^{1/2}}{\tau/\mu-1},\\ \frac{1}{2}(p^2-q^2) &= \frac{2\mu^*/\mu-1}{\tau/\mu-1}.\end{aligned}\right\} \tag{82}$$

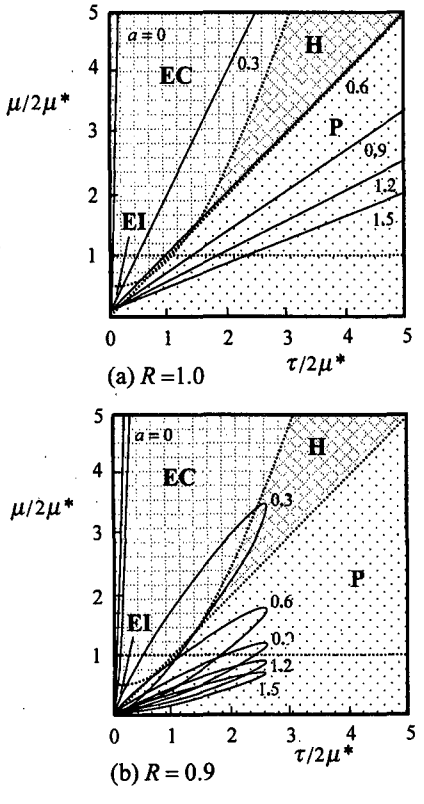

Fig. 6. The $(\tau/2\mu^*, \mu/2\mu^*)$ trajectories with the variation of the material parameter a in (a) the normal-yield state: $R = 1.0$ and (b) the subyield state: $R = 0.9$ for $u_R = 10$.

Fig. 6 represents the bifurcation regimes as a function of dimensionless stress $\tau/2\mu^*$ and moduli ratio $\mu/2\mu^*$ when lateral stress σ_{33} is a constant hydrostatic confining pressure σ_c, and the bifurcation domains coincide for compressive stress. The $(\tau/2\mu^*, \mu/2\mu^*)$ trajectories for several levels of material parameter a ranging from 0.0 to 1.5 in (a) the normal-yield state: $R = 1.0$ and (b) the subyield states: $R = 0.9$ for $u_R = 10$ are depicted in Fig. 6. In case of $R = 1.0$, i.e. near the normal-yield state, the trajectories monotonically rise up to the E-H boundary, whilst the larger material parameter a makes it easier to pass through the boundary with the increase of χ, since both $\tau/2\mu^*$ and $\mu/2\mu^*$ become infinite as the denominator μ^* becomes zero with the increase of χ as was shown in Fig. 5. In case of $R = 0.9$, on the other hand, the $(\tau/2\mu^*, \mu/2\mu^*)$ trajectories first rise up with the increase of χ but they suddenly turn back to the origin, since μ^* does not become zero but inversely increases with the increase of μ^* as was shown in Fig. 5.

Fig. 7 shows the lowest bifurcation stress as a function of the wavelength of the diffuse mode $m\pi a_3/2a_1$ obtained for the symmetric (Fig. 7(a)) and the anti-symmetric (Fig. 7(b)) elliptic modes of bifurcation in several values $2\mu^*/\mu$. The $(\tau/2\mu^*, m\pi a_3/2a_1)$ trajectories for several levels of the normal-yield ratio $R = 0.89$, 0.90 and 1.00 for $u_R = 10$ are depicted in Fig. 7. In case of $R = 1.0$, i.e. near the normal-yield state the trajectories rise up with the increase of $m\pi a_3/2a_1$ and then turn down, whilst in case of subyield states ($R = 0.89$ and $R = 0.9$) the trajectories rise up shortly.

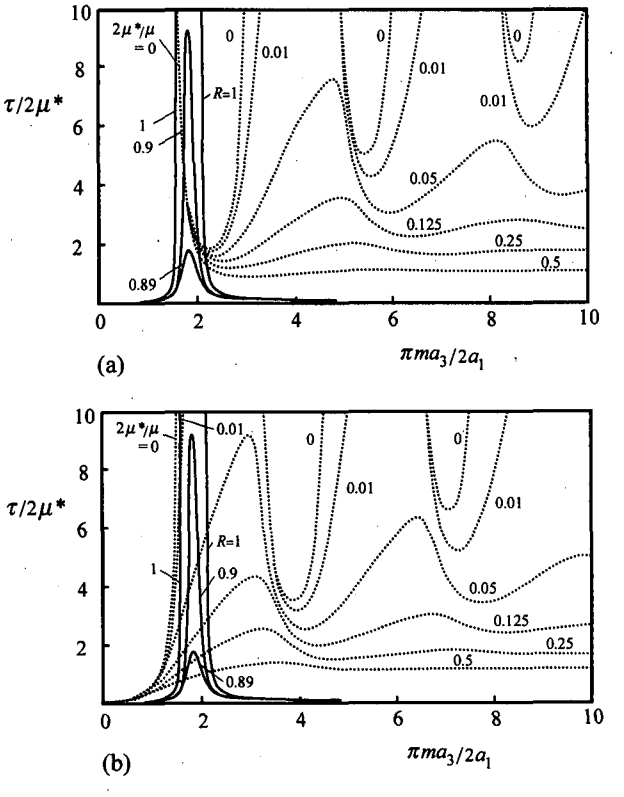

Fig. 7. The $(\tau/2\mu^*, m\pi a_3/2a_1)$ trajectories with variation of R in the lowest bifurcation stress: (a) symmetric modes, (b) anti-symmetric modes.

4. Concluding Remarks

The diffuse bifurcation modes of the rectangular specimen subjected to the undrained plane strain condition are analyzed incorporating the subloading surface model with tangential stress rate effect. The main results obtained in this article are as follows:

1) The analytical solutions for the inception of the diffuse bifurcation modes are derived, which are classified into the elliptic complex, the elliptic imaginary and the hyperbolic and the parabolic regimes.
2) The incorporation of the tangential strain rate has no influence on the instantaneous shear moduli for the normal stress difference but lowers the instantaneous shear moduli for the shear stress.
3) The tangential strain rate term makes easy to fulfill the necessary conditions of bifurcations for not only normal-yield but also subyield states.
4) The formation of symmetric and anti-symmetric bifurcation is affected markedly by the material parameter R in the normal-yield ratio prescribing the approaching degree of the stress to the normal-yield state.

Acknowledgment

The authors would like to express our sincere gratitude to Dr. S. Tsutsumi, Dept. Civil Eng., Tohoku University, for his valuable advices on this analysis. This research has been supported by the Research Fellowships of Ministry of Science, Research and Technology of IRAN.

References

1) Hill, R. and Hutchinson, J., Bifurcation phenomena in the plane tension test, *J. Mech. Phys. Solids*, Vol. 23, pp. 239-264, 1975.
2) Chau, K.T, and Rudnicki, J.W., Bifurcation of compressible pressure-sensitive materials in plane strain tension and compression, *J. Mech. Phys. Solids*, Vol. 38, pp. 875-898, 1990.
3) Young, N. J. B., Bifurcation phenomena in plane compression test. *J. Mech. Phys. Solids*, Vol. 24, pp. 77-91, 1976.
4) Needleman, A., Non-normality and bifurcation in plane strain tension and compression, J. Mech. Phys. Solids, Vol. 27, pp. 231-254, 1979.
5) Vardoulakis, I., Bifurcation analysis of the plane rectilinear deformation on dry sand samples, *Int. J. Solids and Struct.*, Vol. 17, pp. 1085-1101, 1981.
6) Gutierrez, M., Ishihara, K. and Towhata, I., 1991. Flow theory for sand during rotation of principal stress direction, *Soils and Found.*, Vol. 31, pp. 121-132, 1991.
7) Hashiguchi, K. and Tsutsumi, S., Elastoplastic constitutive equation with tangential stress rate effect, *Int. J. Plasticity*, Vol.17, pp. 117-145, 2001.
8) Rudnicki, J.W. and Rice, J.R., Conditions for localization of deformation in pressure-sensitive dilatant materials, *J. Mech. Phys. Solids*, Vol. 23, pp. 371-394, 1975.
9) Yatomi, C., Yashima, A., Iizuka, A. and Sano, I., General theory of shear bands formation by a non-coaxial Cam-clay model, *Soils and Found.*, Vol. 29, pp. 41-53, 1989.
10) Papamichos, E. and Vardoulakis, I., Shear band formation in sand according to non-coaxial plasticity model. *Geotechnique*, Vol. 45, pp. 649-661, 1995.
11) Hashiguchi, K., Fundamental requirements and formulation of elastoplastic constitutive equations with tangential plasticity, *Int. J. Plasticity*, Vol. 9, pp. 525-549. 1993.
12) Hashiguchi, K., Mechanical requirements and struc-tures of cyclic plasticity models, *Int. J. Plasticity*, Vol. 9, pp. 721-748, 1993.
13) Hashiguchi, K., Fundamentals in constitutive equation: continuity and smoothness conditions and loading criterion, *Soils and Found.*, Vol. 40, pp. 155-161, 2000.
14) Hashiguchi, K. and Ueno, M., Elastoplastic constitutive laws of granular materials, *Constitutive Equations of Soils (Proc. 9th Int. Conf. Soil Mech. Found. Eng., Spec. Session 9)*, Tokyo, JSSMFE, pp. 73-82, 1977.
15) Hashiguchi, K., Constitutive equations of elastoplastic materials with elastic-plastic transition, *J. Appl. Mech.* (ASME) Vol. 47, pp. 266-272, 1980.
16) Hashiguchi, K., Subloading surface model in unconventional plasticity, *Int. J. Solids Struct.*, Vol. 25, pp. 917-945, 1989.
17) Hashiguchi, K., Saitoh, K., Okayasu, T. and Tsutsumi, S., Evaluation of typical conventional and unconventional plasticity models for prediction of softening behavior of soils, *Geotechnique*, 52, pp.561-573, 2002.
18) Hashiguchi, K. and Tsutsumi, S., Shear band formation analysis in soils by the subloading surface model with tangential stress rate effect, *Int. J. Plasticity*, Vol. 19, pp, 1651-1677, 2003.

(Received April 18,2003)